

UNCLASSIFIED

UNLIMITED

DATE 1989

2

AD-A213 420



RSRE  
MEMORANDUM No. 4304

# ROYAL SIGNALS & RADAR ESTABLISHMENT

BEAMFORMING PRE-PROCESSORS FOR  
HIGH DISCRIMINATION ALGORITHMS

Author: J L Mather

DTIC  
ELECTE  
OCT 17 1989  
S D

PROCUREMENT EXECUTIVE,  
MINISTRY OF DEFENCE,  
RSRE MALVERN,  
WORCS.

DISTRIBUTION STATEMENT A  
Approved for public release  
Distribution Unlimited

RSRE MEMORANDUM No. 4304

89 10 16 147

UNLIMITED

0051800

CONDITIONS OF RELEASE

BR-111532

\*\*\*\*\*

U

COPYRIGHT (c)  
1988  
CONTROLLER  
HMSO LONDON

\*\*\*\*\*

Y

Reports quoted are not necessarily available to members of the public or to commercial organisations.

ROYAL SIGNALS AND RADAR ESTABLISHMENT

Memorandum 4304

BEAMFORMING PRE-PROCESSORS FOR  
HIGH DISCRIMINATION ALGORITHMS

J L Mather

August 1989

SUMMARY

High discrimination algorithms based on numerical techniques such as eigen analysis are currently being considered for use in future antenna array systems. In addition to being computationally expensive, such algorithms are only able to achieve significantly enhanced within-beam resolution at high signal to noise ratios. However, if the detected signals are found only within a limited frequency range of region of space, or if the data is oversampled, a pre-processing transform may be applied to the data. This leads to a reduction in the size of the data matrix, enables subsequent processing to be accelerated, and lowers the threshold signal to noise ratio required for within-beam resolution. In the spatial domain, the pre-processor is a beamformer. A previous memo has shown how this may be designed using singular vectors of the array calibration matrix. In the current document it is demonstrated by Monte Carlo trials that similar results may be obtained using a conventional beamformer.

Accession For	
NTIS CRAB	<input checked="" type="checkbox"/>
DTIC TAB	<input type="checkbox"/>
Unannounced	<input type="checkbox"/>
Justification	
By	
Distribution	
Availability Codes	
Dist	Avail and/or Special
A-1	

Copyright  
©  
Controller HMSO London  
1989

## CONTENTS

1. INTRODUCTION	1
2. THE DATA MODEL	1
3. METHODS OF DATA ANALYSIS	2
4. BEAMFORMING PRE-PROCESSORS	2
4.1. EIGENVECTOR PROJECTION METHOD (EPM)	2
4.2. CONVENTIONAL BEAMSPACE METHOD (CBM)	3
5. MONTE CARLO SIMULATION RESULTS	3
5.1. INTRODUCTION	3
5.2. DATA COLLECTION AND ANALYSIS	4
5.3. MONTE CARLO RESULTS	4
5.3.1. LINEAR ARRAY	4
5.3.1.1. TWO EQUAL POWER TARGETS CLOSE TO BROADSIDE	4
5.3.1.2. TWO UNEQUAL POWER TARGETS CLOSE TO BROADSIDE	5
5.3.1.3. TARGETS FAR FROM BROADSIDE	5
5.3.1.4. ARRAY CALIBRATION ERRORS	6
5.3.2. POLYGONAL ARRAY	7
6. CONCLUSIONS	7
REFERENCES	7
FIGURES	9

## 1. INTRODUCTION

It is now clear that electrically steered antenna arrays will increasingly replace mechanically aligned dishes in applications ranging from communications and passive detection to active radar and sonar. In addition to advantages such as beam agility and improved reliability, the discrete sampling of the spatial aperture opens up the possibility of sophisticated high discrimination algorithms. Under suitable conditions, such techniques enable the detection of multiple independent signal sources, within the usual aperture-limited beamwidth limitation and below conventional sidelobe levels.

The potential benefits of high discrimination techniques are well recognised. So too are their shortcomings, which include high computational complexity and the requirement of high signal to noise ratios for within-beam resolution. In particular, since many such methods employ eigen analysis of data covariance matrices, the data processing burden is of order  $n^3$  where  $n$  is the number of antenna elements or sub-arrays.

Under certain conditions, as shown in an earlier report [1], by performing additional operations of order  $(k \times n)$ , the dimension of the data covariance matrix may be reduced from  $(n \times n)$  to  $(k \times k)$  where  $k < n$ . The subsequent eigen analysis thus takes  $O(k^3)$  operations, and the overall process may be significantly accelerated. In [1] it was demonstrated that such processing can also enable resolution of two independent signals at fractional beamwidth spacing from lower signal to noise ratios than previously reported. Benefits were also shown for resolution of signals using arrays subject to calibration errors.

The method described in [1] was referred to as an eigenvector projection method (EPM), being based on a transformation of the data using eigenvectors related to the antenna calibration matrix. Its use was illustrated for the case of prior knowledge that all the signals to be detected were confined to a localised region of space. It was shown that, in this case, the transformation is equivalent to a beamforming or spatial filtering operation, and that the improved signal detection capability results from rejection of "out-of-band" noise components. The current report demonstrates that similar results may be obtained using carefully placed conventional beams, and is intended as a supplement to [1].

Section 2 introduces the basic data model. Section 3 reviews the popular MUSIC algorithm [2], and section 4 provides a brief review of EPM (and a similar pre-processor based on conventional beamforming). Section 5 presents a number of experimental results obtained from Monte Carlo trials of algorithms acting on data from a linear array, to illustrate the similar effects of the EPM and beamforming pre-processors. Results obtained using a polygonal array are also included in order to demonstrate the generality of the technique.

## 2. THE DATA MODEL

The usual data model employed [1] is as follows

$$\underline{d}(t) = \mathbf{M} \underline{f}(t) + \underline{x}(t) \quad (1)$$

where  $\underline{f}(t)$  is a vector representing the input which is to be reconstructed,  $\mathbf{M}$  is a linear transformation matrix,  $\underline{x}(t)$  is a vector sample of zero mean Gaussian white noise, and  $\underline{d}(t)$  is the resulting data vector, or "snapshot", at time  $t$ . We assume for simplicity that the matrix  $\mathbf{M}$  (often referred to as the array manifold [2]) is known to within a negligible calibration error [3]. For example, in the case of an array of  $n$  sensors expected to receive signals from independent point sources,  $\mathbf{M}$  will be an  $(n \times N)$  matrix, whose  $N$  columns (denoted  $\underline{m}(\theta_i)$ ,  $i = 1$  to  $N$ ) represent the independent spatial transformations of calibration signals from  $N$  possible discrete angles,  $\theta_i$ . Thus,  $\mathbf{M}$  contains a representative subset of the continuum of possible received waveforms: it provides calibration information about the array rather than details of specific signal sources. If  $\underline{f}(t)$  represents the complex amplitudes of the signals associated with  $m$  independent point sources, as measured at a given instant,  $\underline{d}(t)$  will be given by the linear combination of  $m$  corresponding columns of  $\mathbf{M}$ , scaled by the signal amplitudes and perturbed by additive noise. From a reconstruction of  $\underline{f}(t)$ , we hope to locate the  $m$  sources and estimate their powers.

### 3. METHODS OF DATA ANALYSIS

The usual method of solution is to use the calibration matrix,  $M$ , to form a set of correlation filters which are "matched" to each of the potential signal directions,  $\theta_i$ , and to evaluate

$$P(\theta_i, t) = |f'(\theta_i, t)|^2 = \underline{m}^H(\theta_i) \underline{d}(t) \underline{d}^H(t) \underline{m}(\theta_i) / \{\underline{m}^H(\theta_i) \underline{m}(\theta_i)\}, \quad i = 1 \text{ to } N. \quad (2)$$

The superscript  $H$  denotes the complex conjugate (Hermitian) transpose,  $|\underline{x}|^2$  denotes the squared magnitude of the individual elements of the vector,  $\underline{x}$ , and  $\underline{m}^H(\theta_i)$  is a row of the matrix  $M^H$ . This is a simple estimate of the instantaneous spatial power distribution of the input,  $f(t)$ . Such processing may be considered as "scanning" the data with the beamforming weight vector,  $\underline{m}^H(\theta_i)$ .  $P(\theta, t)$  has the familiar broad multiple lobed pattern of classical analysis, with consequent poor discrimination of multiple signals, resulting from the wide beamwidth and high sidelobes. If a sequence of  $P$  data snapshots has been taken (represented by the matrix  $D$ ), then we may average over time and evaluate

$$P(\theta_i) = \underline{m}^H(\theta_i) D D^H \underline{m}(\theta_i) / \{\underline{m}^H(\theta_i) \underline{m}(\theta_i)\}, \quad i = 1 \text{ to } N. \quad (3)$$

A well-known high discrimination technique, MUSIC [2], makes use of the so-called "noise subspace" eigenvectors,  $E_N$ , corresponding to the  $(n - m)$  smallest eigenvalues of the  $(n \times n)$  covariance matrix,  $(D D^H)$ . The angular estimate is then

$$P(\theta_i) = \frac{\underline{m}^H(\theta_i) E_N E_N^H \underline{m}(\theta_i)}{\underline{m}^H(\theta_i) \underline{m}(\theta_i)}, \quad i = 1 \text{ to } N. \quad (4)$$

The normalisation term in the denominator of equations (2) and (4) allows for non-uniform weighting of the gain vectors represented by the array manifold. The locations of the minima of equation (4) are used to estimate signal directions-of-arrival.

### 4. BEAMFORMING PRE-PROCESSORS

#### 4.1. EIGENVECTOR PROJECTION METHOD (EPM)

In [1] it was shown that, if  $M$  is defined only between angles  $\theta_-$  and  $\theta_+$ , then the matrix  $(M M^H)$  has approximately  $k$  large eigenvalues, where  $k$  is the angle  $(\theta_+ - \theta_-)$  measured in conventional beamwidths. The  $k$  corresponding eigenvectors, denoted  $U_k$ , may be used as a pre-processing transformation of the data. The validity of such processing rests on the assumption that the signal components in the data matrix may be sufficiently accurately represented by the  $(k \times P)$  matrix

$$C = U_k^H D. \quad (5)$$

Thus, we assume that components of the data which are suppressed by this projection are indistinguishable from noise. This is the basis of the eigenvector projection method (EPM).

Clearly, finding  $E$  for use in equation (4) imposes a heavy processing burden if the sensor array dimension  $n$  is large. If  $k \ll n$ , the noise subspace eigenvectors,  $F_N$ , of the modified data covariance matrix  $(C C^H)$  may be evaluated much more rapidly. A bounded solution can then be calculated, via the MUSIC algorithm, as

$$P(\theta_i) = \frac{\underline{m}^H(\theta_i) U_k F_N F_N^H U_k^H \underline{m}(\theta_i)}{\underline{m}^H(\theta_i) U_k U_k^H \underline{m}(\theta_i)}, \quad i = 1 \text{ to } N', \quad \theta_- < \theta_i < \theta_+. \quad (6)$$

Here,  $U_k$  transforms the vectors  $F_N$  back into the  $n$ -space of the array manifold.  $N'$  may be less than  $N$  without loss of detail, since  $\theta_+$  and  $\theta_-$  are less than the maximum possible non-ambiguous angles of arrival. Correct normalisation is maintained by using the "modified" array manifold vectors,  $U_k^H \underline{m}(\theta_i)$ , in the denominator. This is particularly important in the use of EPM with certain other algorithms, such as Burg's MEM [4] and the method of Kumaresan and Tufts [5]. Further details may be found in [1].

Signal powers and time-domain behaviour may be estimated [1,3] simply by replacing  $M$  in the usual equations by  $A = (U_k^H M)$ . Each identified signal direction is referenced to a

particular column of  $\mathbf{A}$ . If these columns are collected together and stored in a matrix  $\mathbf{A}_s$ , the time series associated with each direction is a row of the matrix  $\mathbf{T}$ , given by [1,3]

$$\mathbf{T} = (\mathbf{A}_s^H \mathbf{A}_s)^{-1} \mathbf{A}_s^H \mathbf{C} \quad (7)$$

and the signal powers may be estimated as the diagonal elements of the matrix

$$\mathbf{P} = \mathbf{T} \mathbf{T}^H \quad (8)$$

If we assume that the additive noise,  $\underline{\mathbf{w}}(t)$ , is spatially uncorrelated or "white", then, since the operation defined by equation (5) is equivalent to spatial filtering [1], EPM pre-processing will lead to a reduction in the total noise power in the data. As the Monte Carlo simulation results described in [1] show, EPM pre-processing leads to more accurate angular estimates as a result of this noise reduction. There is an improvement in both the fidelity of extracted time series and the accuracy of the estimated powers, over results from the equivalent "conventional" high discrimination processing. This occurs principally at low signal to noise ratio, by virtue of the enhanced probability of resolution.

#### 4.2. CONVENTIONAL BEAMSPACE METHOD (CBM)

EPM is equivalent to a spatial beamforming process, using the conjugate transpose of the principal eigenvectors,  $\mathbf{U}_k^H$ , of  $(\mathbf{M} \mathbf{M}^H)$  in place of the usual beam steering vectors represented by columns,  $\underline{\mathbf{m}}(\theta_i)$ , of  $\mathbf{M}$ . For the example of a linear antenna array with 16 equi-spaced elements, the vectors  $\underline{\mathbf{m}}(\theta_i)$  have the form of truncated complex exponentials (Fig. 1), and produce the "sinc" shaped beams illustrated in Fig. 2. The vectors  $\mathbf{U}_k$  are discrete prolate spheroidal functions [6] and are shown in Fig. 3 for the same array. The "beams" contributed by the eigenvectors each have a different pattern (Fig. 4).

If only a limited number of conventional beams or eigenvector beams are formed and summed, the resulting overall beam patterns will differ. Fig. 5 illustrates this. Fig. 5a shows a typical function applied to the data space by EPM. It assumes a 4 beamwidth angular region of interest, using a 16 element 0.5 wavelength spaced linear array, and  $k = 5$ . Fig. 5b shows the function obtained using five equally weighted conventional beams, directed at  $-1.78$ ,  $-0.89$ ,  $0$ ,  $0.89$  and  $1.78$  beamwidths away from boresight. These positions have been chosen such that the resulting pattern approximately resembles that of the eigenvector processor. In filter terms, the choice of beam positions gives a trade-off between in-band ripple and out-of-band rejection. We have not explored the effect of using differently weighted or irregularly spaced beams. EPM has the advantage of providing a secure basis for choosing the optimal maximum number of "beams", based on knowledge of signal to noise. EPM also automatically places the "beams" to give a smooth "in-band" response.

Although the angular estimates of signals, derived following EPM or CBM pre-processing, are insensitive to the validity of the assumed angular frequency constraints,  $\theta_-$  and  $\theta_+$ , the same is not true of the signal extraction and power estimation stages (equations (7) and (8)). If significant signal amplitudes exist at unknown angles beyond these boundaries, the estimates of power and time behaviour may degrade [1]. This is true for any high discrimination algorithm which fails to locate one or more signals accurately, and is a feature of the power estimation step rather than the angle estimation per se. It should be possible to reduce such sensitivity by applying constrained adaptive cancellation techniques to null signals in the sidelobes of the EPM filter during power estimation.

### 5. EXPERIMENTAL RESULTS

#### 5.1. INTRODUCTION

The experimental results presented here confirm that both EPM and CBM can be designed to give approximately equivalent benefit to the subsequent parameter estimation algorithm. The results are taken from a series of Monte Carlo trials of well-known algorithms, acting in combination with each of the pre-processors on simulated data. To emphasise the generality of these methods, both linear and polygonal sensor arrays have been simulated.

In section 5.2, the collection and analysis of the Monte Carlo data is outlined. Section 5.3 describes results obtained from analyses of data generated from a variety of typical two source scenarios. Results obtained from high discrimination algorithms acting on the normal covariance matrix are compared to those obtained from the same algorithms acting on the reduced size covariance matrix output from EPM or CBM. A more comprehensive set of results for EPM is presented in [1].

## 5.2. DATA COLLECTION AND ANALYSIS

Monte Carlo simulations enable comparison of the performance of algorithms, with and without EPM or CBM, over many trials. Results are collected in terms of such parameters as the bias and standard deviation of the angle and power estimates, the probability of resolution and false alarm rate. Statistics are based on 100 trials of each algorithm at each of a number of discrete angular separations and signal to noise ratios. The results are presented in the same format as those of [1].

Fig. 6 is a summary of the procedure used in the collection and analysis of the statistical data. During the Monte Carlo trials, the positions of all estimated angles of arrival are recorded, together with the corresponding powers. When analysing this data, thresholds may be set in angle or power in order to distinguish between correctly identified signals, false alarms, and estimates which may be ignored. For example, Fig. 7 shows how thresholds may be set in power and angle. Firstly a noise level power threshold is set, all signals falling below this line being rejected. Signals above this threshold are assigned as detections if the estimate of (angle, power) falls within the window defined by an angular uncertainty,  $\Delta\theta$ , and a power uncertainty,  $\Delta P$ , each centred on the appropriate true signal coordinate. All other detections are counted as false alarms. The statistical results presented in the following sub-sections are all conditioned on resolution (detection of both targets), as indicated in Fig. 6.

In the following sections, signal to noise ratio is measured in terms of the "array signal to noise ratio" (ASNR) of one of the two targets. This is defined as ((instantaneous signal to noise ratio at each element of the array) -  $10 \log_{10}(n)$ ).

## 5.3. MONTE CARLO RESULTS

### 5.3.1. LINEAR ARRAY

The results presented in Figs. 8 to 18 relate to the analysis of multiple snapshots of data from a 16 element linear array with 0.5 wavelength element spacing. The dimension  $k$  chosen for both the EPM and CBM pre-processors is equal to 5 throughout. The target scenario consists of two random phase signal sources in the far field, separated by a fractional beamwidth. This beamwidth is the angle from the peak of the main lobe of a matched filter (equation (2)) at the first target location, to the position of its first null.

#### 5.3.1.1. TWO EQUAL POWER TARGETS CLOSE TO BROADSIDE

In this section,  $\theta_+$  and  $\theta_-$  are set to  $\pm 14.5^\circ$  ( $\pm 4$  beamwidths), and the equal power signals are located at broadside (perpendicular to the array) and at 0.1 beamwidths to one side.

Fig. 8 shows the variation of the performance statistics as a function of ASNR (the theoretical integrated signal to noise power ratio for each of the two emitters). 16 snapshots of data have been used for each trial. The results, taken at 3dB signal to noise ratio increments, are shown for the MUSIC algorithm acting on the  $16 \times 16$  covariance matrix (dot-dash lines) and for MUSIC acting on the EPM and CBM processed  $5 \times 5$  covariance matrices (dotted and dashed lines, respectively). The solid line in the plot of standard deviation is the Cramér Rao bound [7] for the problem, assuming uncorrelated emitters. A noise power threshold of  $10 \log_{10}(n)$  has been used, together with  $\Delta\theta = 1$  beamwidth and  $\Delta P = 6\text{dB}$  (see Fig. 7).

In all three cases, as the ASNR rises, the probability of resolution increases (associated with a peak in the false alarm rate), bias of the angle and power estimates tend to zero,

and the variance of the angle estimates,  $\text{var}(\hat{\theta}_i)$ , tend towards the Cramér Rao bound. The bias and variance results are plotted for the "left-hand" signal, and thus negative angular bias indicates that the nulls of  $P(\theta)$  corresponding to the signals have moved further apart.

In addition to reducing the time taken for the computation of the eigenvectors by a factor of approximately 32, we see that processing by either EPM or CBM has an effect on performance which is roughly equivalent to a 5-10dB increase in array signal to noise ratio. If the noise was distributed equally amongst all the available degrees of freedom (and the signal was concentrated in the  $k$  primary degrees of freedom) before processing by EPM or CBM, we might expect an improvement of approximately 5dB in this case, and so the observed change seems reasonable. The behaviour of EPM/MUSIC is virtually indistinguishable from that of CBM/MUSIC for the current choice of beam positions.

Fig. 9 shows a similar set of results to those of Fig. 8, for the case in which only 5 snapshots of data have been collected.

### 5.3.1.2. TWO UNEQUAL POWER TARGETS CLOSE TO BROADSIDE

High discrimination algorithms, of the type referred to in this report, enable the detection of multiple signals within the beamwidth defined by the matched filter (equation (2)), and, perhaps even more importantly, also allow the detection of targets whose powers fall below the sidelobes of the conventional beamformer. We further expect to be able to resolve signals of differing powers within the main beamwidth.

Fig. 10 compares the performance of MUSIC with that of EPM( $k=5$ )/MUSIC and CBM( $k=5$ )/MUSIC acting on 16 snapshots of data. There are two signals, located at 0 and 0.1 beamwidths with respect to broadside.  $\theta_+$  and  $\theta_-$  are again set to  $\pm 14.5^\circ$  ( $\pm 4$  beamwidths). In this case, the ratio of the power of the signal at broadside to that of the signal at 0.1 beamwidths is -20dB, and the ASNR scales in Fig. 10 correspond to the lower power signal.

As in the previous section, the performance of the basic algorithm is improved through the application of either EPM or CBM, by the equivalent of between 5 and 10dB ASNR. It can be seen from comparison with Fig. 8, for equal power signals, that there has been a slight deterioration in overall performance for all three implementations in the present case. The false alarm rate is slightly higher and the probability of resolution curve falls to zero at slightly higher ASNR than in Fig. 8.

### 5.3.1.3. TARGETS FAR FROM BROADSIDE

Because the assumption that signals are confined to a region about the broadside position is similar to one of spatial oversampling, it may appear strange to consider using EPM for a field of view in which such oversampling cannot be assumed. However, looked at as a spatial beamforming operation, this clearly should be possible. Thus, the singular values of a calibration matrix limited by  $\theta_- = 30^\circ$  and  $\theta_+ = 90^\circ$  (a span of 4 beamwidths for the 16 element linear array) decline in a similar way to those of a calibration limited by  $-\theta_- = \theta_+ = 14.5^\circ$  (4 beamwidths). Again, the maximum number of "significant" basis vectors,  $U_k$ , can be determined from knowledge of the overall signal to noise ratio, and an EPM filter defined. Fig. 11a shows the EPM spatial filter function created by taking  $k = 5$ . The function is not as sharply confined to the region of interest as was the case in Fig. 5a. However, if the assumed angle of view is valid, then this will not be a problem. A CBM pre-processor may also be defined, using 5 conventional beams. In the design used here, which has the spatial response shown in Fig. 11b, the beams are directed at 4.2, 5.15, 6.1, 7.05 and 8 beamwidths from broadside.

Taking the above calibration, with two equal power independent sources located at 7.7 and 7.9 beamwidths ( $74.3^\circ$  and  $80.9^\circ$ ) from broadside, Fig. 12 compares the performance of MUSIC acting on the full 16x16 covariance matrix with that achievable via the 5x5 processed covariance estimates. Probability of resolution has improved as a result of the EPM pre-processing, although by the equivalent of only a 2-3dB shift along the ASNR axis, which is somewhat less than was the case for targets close to broadside. Probability

of resolution when using CBM starts to increase at lower ASNR, but requires greater signal power to reach 100%. In both cases, variance of the angle estimate has actually increased. A more careful design of the CBM pre-processor could possibly match the performance of EPM.

We note that the experiments described in [1] showed that behaviour in this far-from-broadside region was strongly dependent on the high discrimination algorithm employed. It was found for example, that the performance of MEM [4] could be significantly improved by EPM. We should therefore also expect some improvement from use of CBM.

#### 5.3.1.4. ARRAY CALIBRATION ERRORS

The particular high discrimination algorithms referred to in this report are known to be sensitive to errors in the calibration of the antenna array, embodied in the matrix  $\mathbf{M}$ . Thus further simulations were carried out to investigate the effect of EPM pre-processing under such circumstances. Data consisted of 16 snapshots from a 16 element linear array, as in previous sections, but with random calibration errors of  $\pm 10\%$  in amplitude and  $\pm 1\%$  in phase across the elements. These errors were chosen from independent rectangular distributions. The particular weight set used for these simulations is given in Fig. 13.

For illustration in the present section, Figs. 14 and 15 show results obtained for two equal power signals, located at 0 and 0.2 beamwidths away from broadside. Algorithms used on the data from the mis-calibrated array were MLM [8,1], EPM( $k=5$ )/MLM [1] and CBM( $k=5$ )/MLM for Fig. 14 and MUSIC, EPM( $k=5$ )/MUSIC and CBM( $k=5$ )/MUSIC for Fig. 15. The field of view extended to  $\pm 14.5^\circ$ . The beams used by CBM were designed from the assumed (error-free) calibration, rather than that used for generation of data.

The presence of errors in the array calibration has caused the performance of MLM (Fig. 14) to deteriorate considerably. Probability of resolution reaches only around 0.5 for ASNRs less than 60dB; false alarm rate is higher than in the accurately calibrated case (as can be seen from results presented in [1]) and continues to rise with increasing ASNR; standard deviation of the angle estimates declines only gradually with increasing ASNR; and there is an almost constant bias of both the angle and power estimates. Pre-processing using either EPM or CBM increases probability of resolution to greater than 0.9 by 40dB ASNR, reduces the false alarm rate for the same thresholding procedure (although the trend is still rising as ASNR increases), and reduces both standard deviation and bias. Power estimation variance remains virtually unchanged after pre-processing.

Under the same circumstances, Fig. 15 shows MUSIC to be more robust, in that it is still possible to achieve 100% probability of resolution, and variance of the angle estimates remains close to the Cramér Rao bound. Both EPM and CBM confer further gains in performance.

An alternative representation of some of this data is given in Figs. 16 to 18. These take the form of scatter diagrams. These represent power and angle estimates taken at selected ASNRs, using MUSIC (Fig. 16), MLM (Fig. 17) and EPM/MLM (Fig. 18). True signal coordinates are denoted by "O", whilst estimated coordinates are indicated by dots. Thus, in Fig. 16, for example, the first panel shows the approximately uniform scatter of estimates for the case of both  $(p_1, \theta_1)$  and  $(p_2, \theta_2)$  equal to  $(0\text{dB}, 1.43^\circ)$ , a separation of 0.2 beamwidths. Both signals are effectively indistinguishable from noise. As signal powers increase, the estimates cluster more tightly, close to the true signal coordinates. The bias of both angle and power estimates is clearly depicted. Fig. 17 clearly indicates the almost constant variance with increasing ASNR which characterises the results from MLM, and Fig. 18 shows how this is reduced if EPM is used to pre-process the data.

It is worth noting that the results described here have been collected for a single perturbed antenna calibration. More work needs to be carried out before general conclusions regarding the relative robustness of algorithms can be derived with certainty.

### 5.3.2. POLYGONAL ARRAY

In order to emphasise the generality of the EPM and CBM techniques, Figs. 20 and 21 show results obtained using MLM and MUSIC, and their pre-processed counterparts acting on 16 snapshots of data from a 16 element circular array with a radius of 1.33 wavelengths. The characteristics of the EPM( $k=5$ ) and CBM( $k=5$ ) beamformers are shown in Fig. 19. The angular inter-beam separation chosen for CBM was  $18^\circ$ .

Fig. 20 shows results obtained using MLM, EPM/MLM and CBM/MLM for the case of two equal powered signals separated by 0.1 beamwidths (2.25 degrees). Fig. 21 shows the performance of MUSIC, EPM/MUSIC and CBM/MUSIC under the same circumstances. Algorithm behaviour is clearly similar to that observed with linear arrays (section 5.3.1.1).

## 6. CONCLUSIONS

A substantial reduction may be achieved in the processing time required by modern high resolution algorithms. This is achieved by means of a beamforming pre-processor. Design of this processor may make use of eigenvectors related to the array manifold, or carefully directed conventional beams. The eigen-based method, EPM, removes the need to make decisions regarding beam placement and weighting, through the use of an information theoretic result [1]. In addition, the Monte Carlo results have demonstrated that such pre-processing can significantly improve the ability of a number of high discrimination algorithms to extract signal parameters from noisy data. Furthermore, beamforming pre-processing has been observed to have a beneficial effect on data taken from an array whose calibration was randomly perturbed. Finally, we have demonstrated, using a non-linear array, that such processing is equally applicable to alternative array geometries.

## REFERENCES

- [1] Mather, J.L.  
A Monte Carlo performance analysis of accelerated svd-based high discrimination algorithms.  
Royal Signals and Radar Establishment Memorandum no. 4083. (1988).
- [2] Schmidt, R.O.  
Multiple emitter location and signal parameter estimation.  
RADC Spectrum Estimation Workshop, 243-258, (1979).
- [3] Mather, J.L.  
Least squares solutions in signal processing using the singular value decomposition.  
Royal Signals and Radar Establishment Memorandum no. 3864, (1986).
- [4] Burg, J.P.  
The relationship between maximum entropy spectra and maximum likelihood spectra.  
Geophysics **37**(2), 375-376, (1972).
- [5] Kumaresan, R., Tufts, D.W.  
Estimating angles of arrival of multiple plane waves.  
IEEE Trans. AES-**19**(1), 134-139, (1983).
- [6] Slepian, D.  
Prolate spheroidal wave functions, Fourier analysis, and uncertainty - V: The discrete case.  
Bell Syst. Tech. J. **57**(5), 1371-1430, (1978).
- [7] van Trees, H.L.  
Detection, estimation, and modulation theory, I.  
Wiley, N.Y., 1968.
- [8] Capon, J., Greenfield, R.J., Kolker, R.J.  
Multidimensional maximum likelihood processing of a large aperture seismic array.  
Proc. IEEE **55**(2), 192-211, (1967).



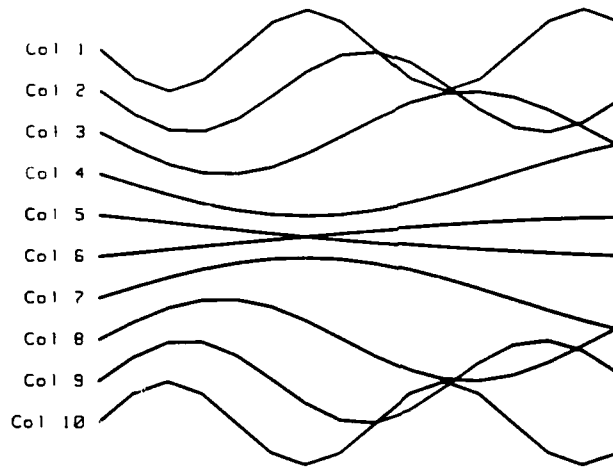


Fig. 1. A selection of typical calibration vectors for a linear array of 16 elements, spaced by 0.5 wavelengths, corresponding to plane wave signals detected at the array. Only the imaginary components are shown.

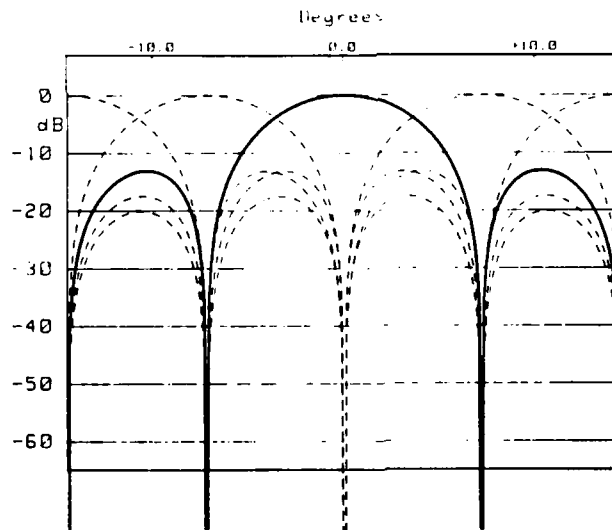


Fig. 2. The far-field beamshapes corresponding to five of the calibration vectors shown in Fig. 1. The beams are directed at  $-2$ ,  $-1$ ,  $0$ ,  $1$ , and  $2$  beamwidths from broadside. The central beam is represented by the solid line, and the rest by dashed lines for clarity. The patterns are plotted over a field of view of 4 beamwidths, centred on broadside.

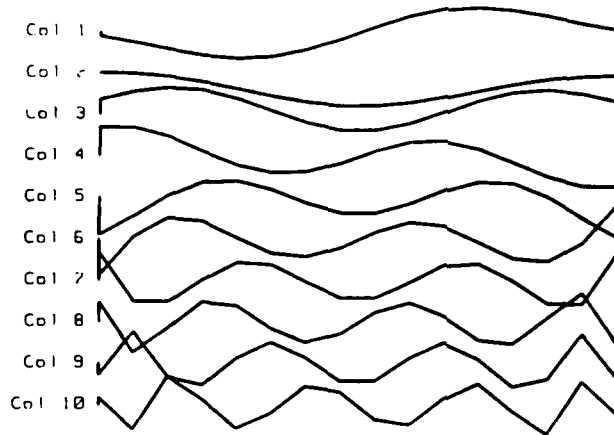


Fig. 3. The first 10 eigenvectors of the matrix  $(M M^H)$ , where  $M$  is the calibration matrix for the 16 element linear array shown in Fig. 1. These correspond to the 10 largest eigenvalues of  $(M M^H)$ .

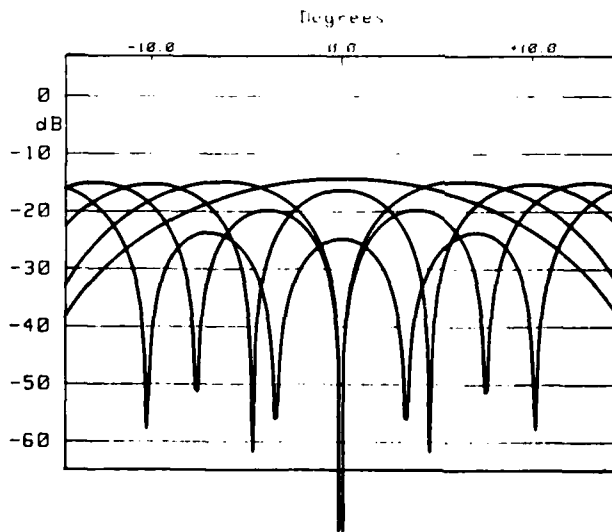


Fig. 4. Far-field beam patterns corresponding to the first five individual eigenvectors shown in Fig. 3. The patterns are plotted over a field of view of 4 beamwidths, centred on broadside.

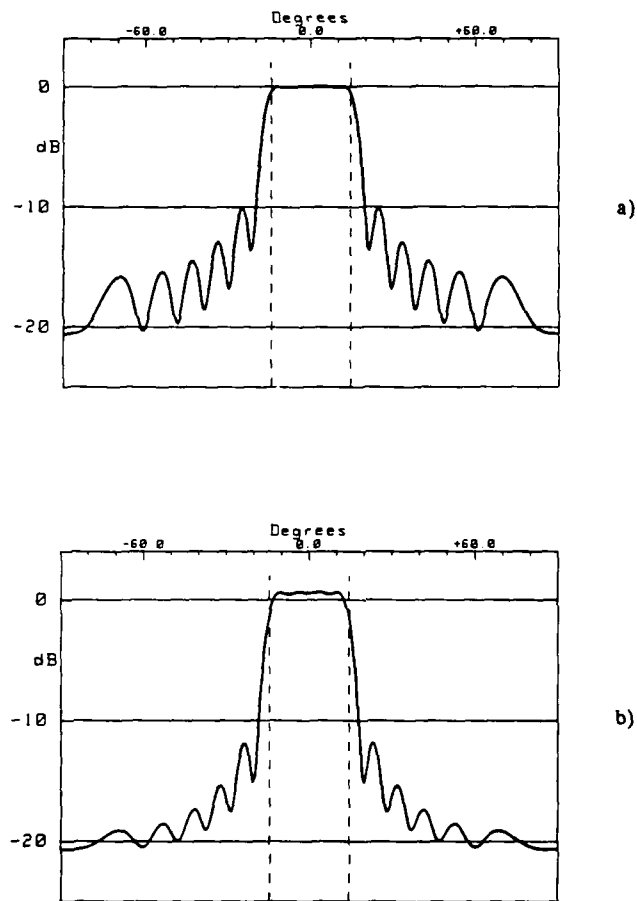


Fig. 5. (a) Spatial frequency filter function applied by EPM( $k=5$ ), assuming angular constraints given by  $\sin(\theta_+) = -\sin(\theta_-) = 0.25$  (indicated by vertical broken lines) for a 16 element 0.5 wavelength spaced linear array. (b) Spatial filter function obtained using 5 equally weighted conventional beams, directed at  $-1.667$ ,  $-0.833$ ,  $0$ ,  $0.833$ , and  $1.667$  beamwidths away from broadside.

## DATA COLLECTION AND ANALYSIS ALGORITHM

```

1. RECORD DATA:
  FOR each emitter separation
    FOR each signal to noise ratio
      FOR each repeat
        generate new data matrix
        FOR each algorithm
          RECORD angle and power estimates onto disc
        NEXT algorithm
      NEXT repeat
    NEXT signal to noise ratio
  NEXT emitter separation

2. ANALYSE DATA:
  FOR each separation
    FOR each signal to noise ratio
      FOR each repeat
        FOR each algorithm
          FOR each angle estimate
            test against thresholds in angle and power
            assign targets to estimates
            record positions and powers of resolved pairs
          NEXT angle estimate
          count total false alarms
          count total resolutions
        NEXT algorithm
      NEXT repeat
    FOR each algorithm
      average probability of resolution
      average false alarm rate
    NEXT algorithm
  NEXT signal to noise ratio
  FOR each signal to noise ratio
    FOR each algorithm
      FOR each emitter
        IF resolved THEN
          calculate mean position
          calculate mean power
          calculate bias of mean from true position
          calculate bias of power estimate
          calculate standard deviation of angle estimates
          calculate standard deviation of power estimates
        END IF
      NEXT emitter
    NEXT algorithm
  NEXT signal to noise
NEXT separation

```

Fig. 6. Monte Carlo data collection and analysis procedures.

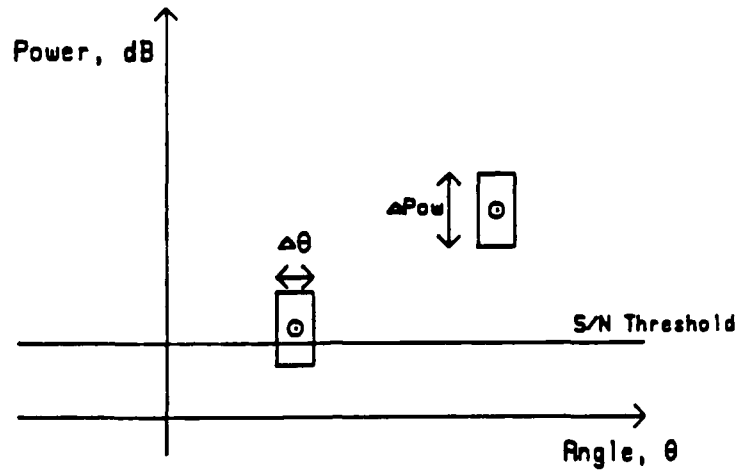


Fig. 7. Two signals are indicated by  $\odot$  symbols. During data analysis, a power threshold may be set, below which all estimates are assumed to be related to noise and are therefore ignored. All estimates above this signal to noise threshold are then counted as either false alarms or true target detections. Signals are assumed to be detected if the (angle, power) coordinates fall within the boxes defined by the true signal coordinates, and  $\Delta\theta$  and  $\Delta\text{Pow}$ . Throughout the analyses presented in the present report,  $\Delta\theta = 1$  beamwidth, and  $\Delta\text{Pow} = 6\text{dB}$ .

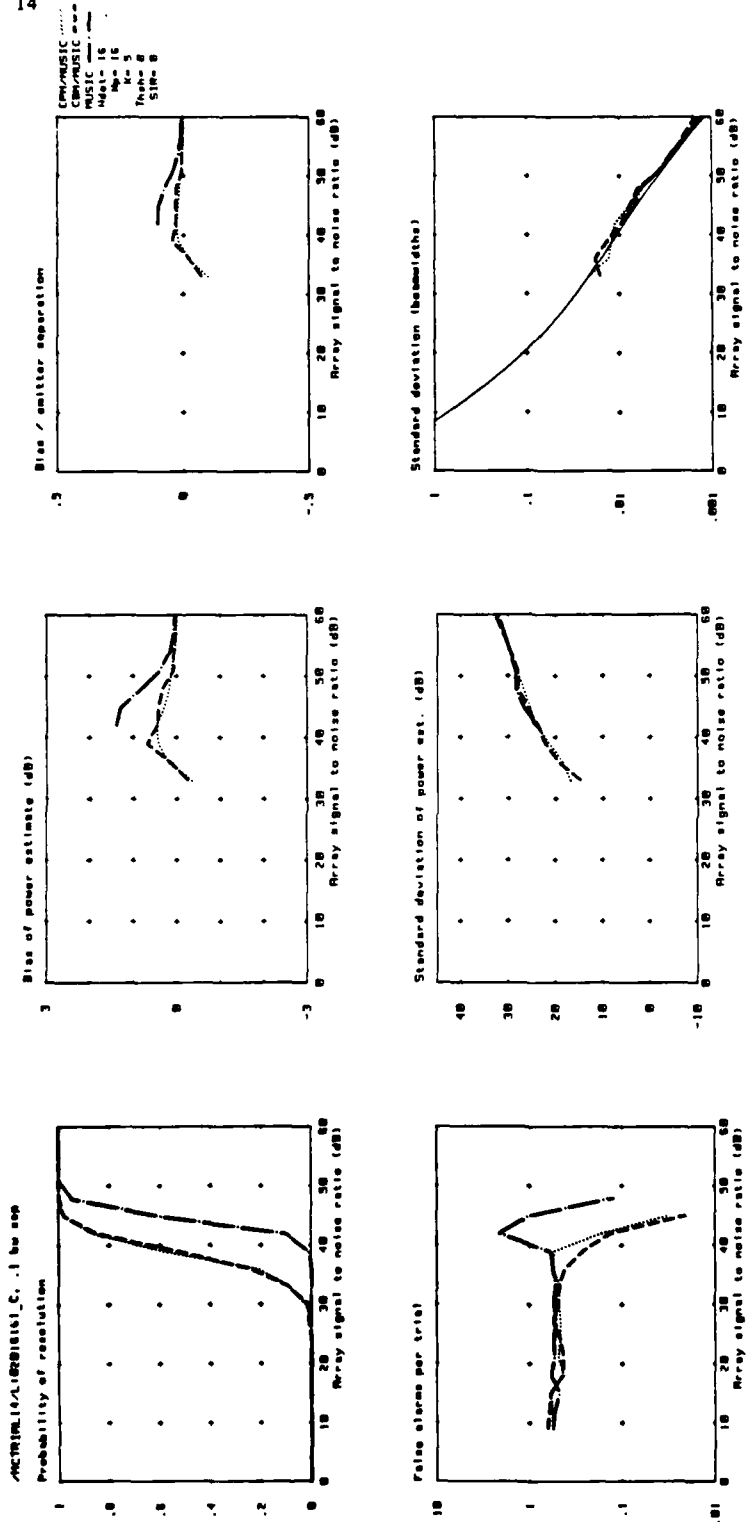


Fig. 8. Performance statistics as a function of array signal to noise ratio (ASNR) for two equal power signals, located at 0 and 0.1 beamwidths from broadside. Results are based on 100 trials at each ASNR, taking 16 snapshots of data from the 16 element 0.5 wavelength spaced linear array. Dot-dashed lines show the results of processing using the MUSIC algorithm (equation (9)), dotted lines show the results obtained using EPM(k=5)/MUSIC, and dashed lines show the results obtained using Cramer Rao bound. Assumed angle of view from -2 to +2 beamwidths. The continuous line in the plot of angular standard deviation is the Cramer Rao bound.

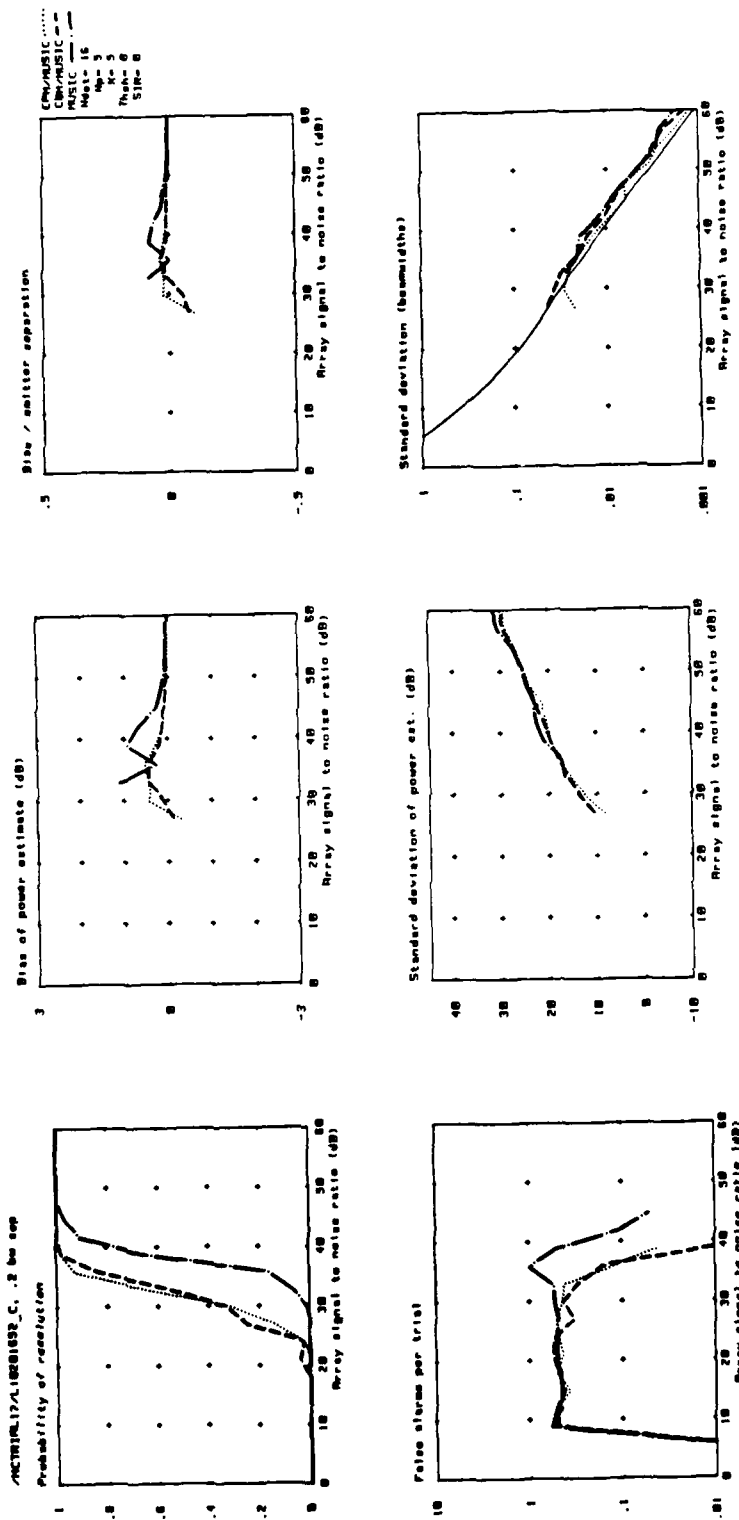


Fig. 9. Performance statistics as a function of array signal to noise ratio (ASNR) for two equal power signals, located at 0 and 0.1 beamwidths from broadside. Results are based on 100 trials at each ASNR, taking 5 snapshots of data from the 16 element 0.5 wavelength spaced linear array. Dot-dashed lines show the results of processing using the MUSIC algorithm (equation (4)), dotted lines show the results obtained using EPM(k=5)/MUSIC, and dashed lines show the results obtained using CBM(k=5)/MUSIC. Assumed angle of view from -2 to +2 beamwidths. The continuous line in the plot of angular standard deviation is the Cramér Rao bound.

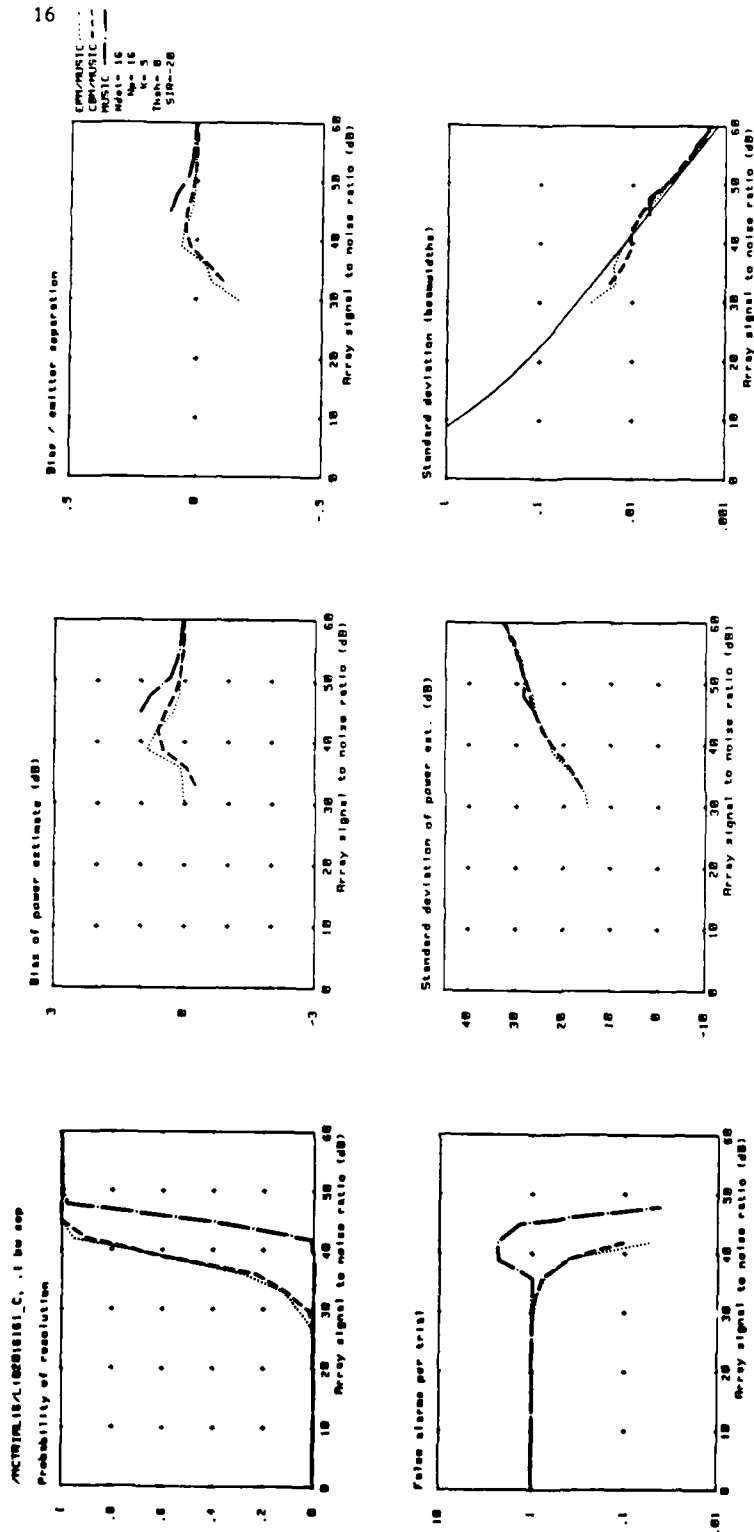


Fig. 10. Performance statistics as a function of array signal to noise ratio (ASNR) for two unequal power signals, located at 0 and 0.1 beamwidths from broadside. The ASNR scale corresponds to the lower power signal, which has a power 20dB lower than the off-broadside signal. Results are based on 100 trials at each ASNR, taking 16 snapshots of data from the 16 element 0.5 wavelength spaced linear array. Dot-dashed lines show the results of processing using the MUSIC algorithm (equation (4)). Dotted lines show the results obtained using EPM(k=5)/MUSIC, and dashed lines show the results obtained using CBM(k=5)/MUSIC. Assumed angle of view from -2 to +2 beamwidths. The continuous line in the Plot of angular standard deviation is the Cramér Rao bound.

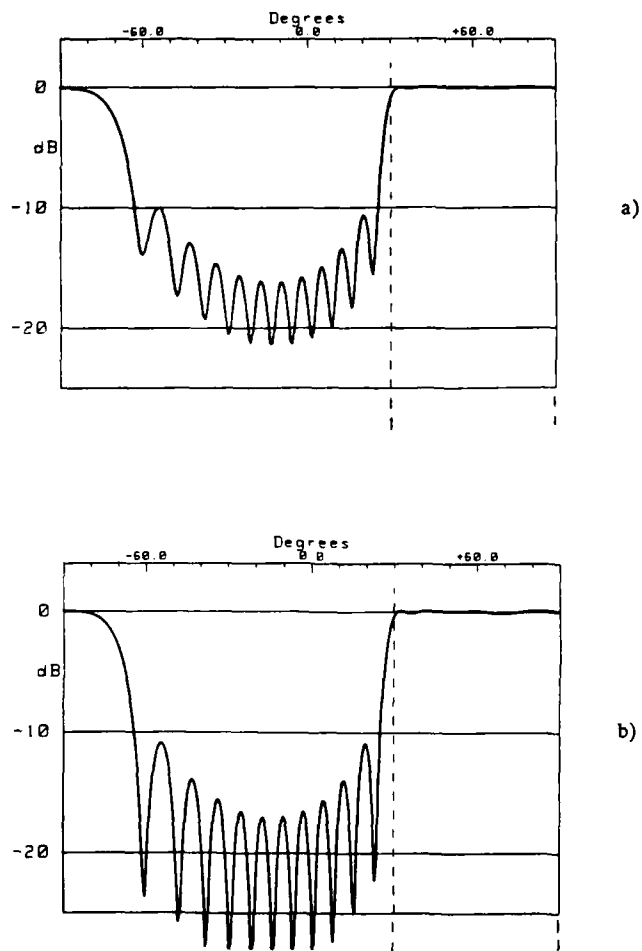


Fig. 11. a) Spatial frequency filter function applied to data by EPM( $k=5$ ), assuming angular constraints given by  $\sin(\theta_-) = 0.5$  and  $\sin(\theta_+) = 1.0$  (indicated by vertical broken lines) for a 16 element 0.5 wavelength spaced linear array. b) Spatial frequency filter function applied to data by CBM( $k=5$ ), for the same array. Beams have been directed at 4.2, 5.15, 6.1, 7.05, and 8 beamwidths from broadside.

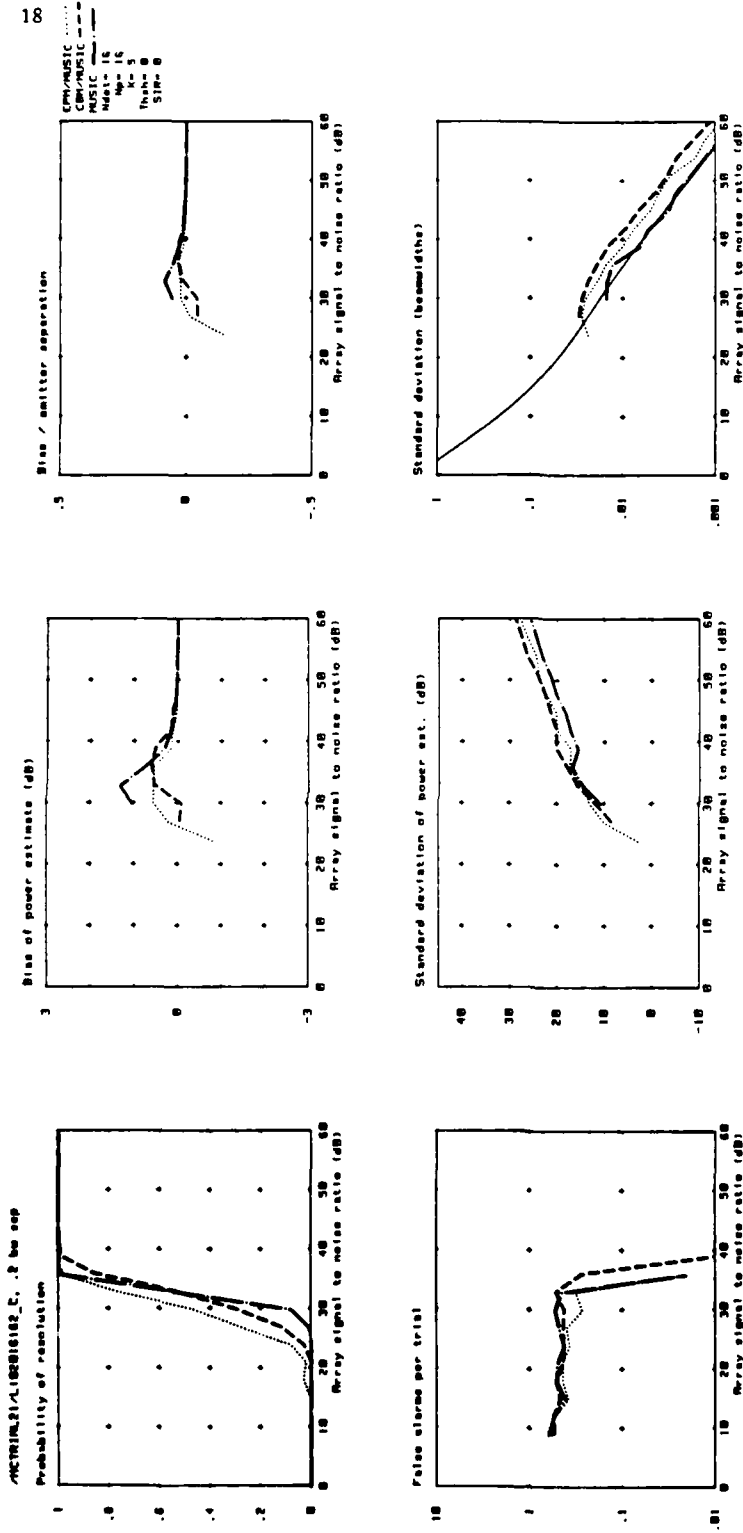


Fig. 12. Performance statistics as a function of array signal to noise ratio (ASNR) for two signals, located at 7.7 and 7.9 beamwidths from broadside. Results are based on 100 trials at each ASNR, taking 16 snapshots of data from the 16 element 0.5 wavelength spaced linear array. Dot-dashed lines show the results of processing using the MUSIC algorithm (equation (4)), dotted lines show the results obtained using EPM(k=5)/MUSIC, and dashed lines show the results obtained using CBM(k=5)/MUSIC. Assumed angle of view from +4 to +8 beamwidths.

<u>Element</u>	<u>assumed amplitude</u>	<u>assumed phase (rads)</u>	<u>perturbed amplitude</u>	<u>perturbed phase (rads)</u>
1	1.0	0.0	0.917188	-1.204603×10 <sup>-2</sup>
2	1.0	0.0	0.978620	4.648638×10 <sup>-2</sup>
3	1.0	0.0	1.072075	-1.910583×10 <sup>-2</sup>
4	1.0	0.0	0.934826	1.410884×10 <sup>-2</sup>
5	1.0	0.0	0.999926	-2.143270×10 <sup>-2</sup>
6	1.0	0.0	1.092877	-0.472322×10 <sup>-2</sup>
7	1.0	0.0	1.057702	0.350052×10 <sup>-2</sup>
8	1.0	0.0	1.036057	0.536220×10 <sup>-2</sup>
9	1.0	0.0	1.034596	3.968480×10 <sup>-2</sup>
10	1.0	0.0	0.935603	4.797734×10 <sup>-2</sup>
11	1.0	0.0	0.954129	3.087766×10 <sup>-2</sup>
12	1.0	0.0	0.951808	2.046928×10 <sup>-2</sup>
13	1.0	0.0	0.936404	-3.966099×10 <sup>-2</sup>
14	1.0	0.0	0.901499	-5.989737×10 <sup>-2</sup>
15	1.0	0.0	0.994882	-1.169561×10 <sup>-2</sup>
16	1.0	0.0	0.952047	3.292482×10 <sup>-2</sup>

Fig. 13. Assumed and actual array calibrations used to demonstrate sensitivity of algorithms to calibration error. The errors are uniformly distributed, and correspond to a maximum of ±10% in amplitude and ±1% in phase.

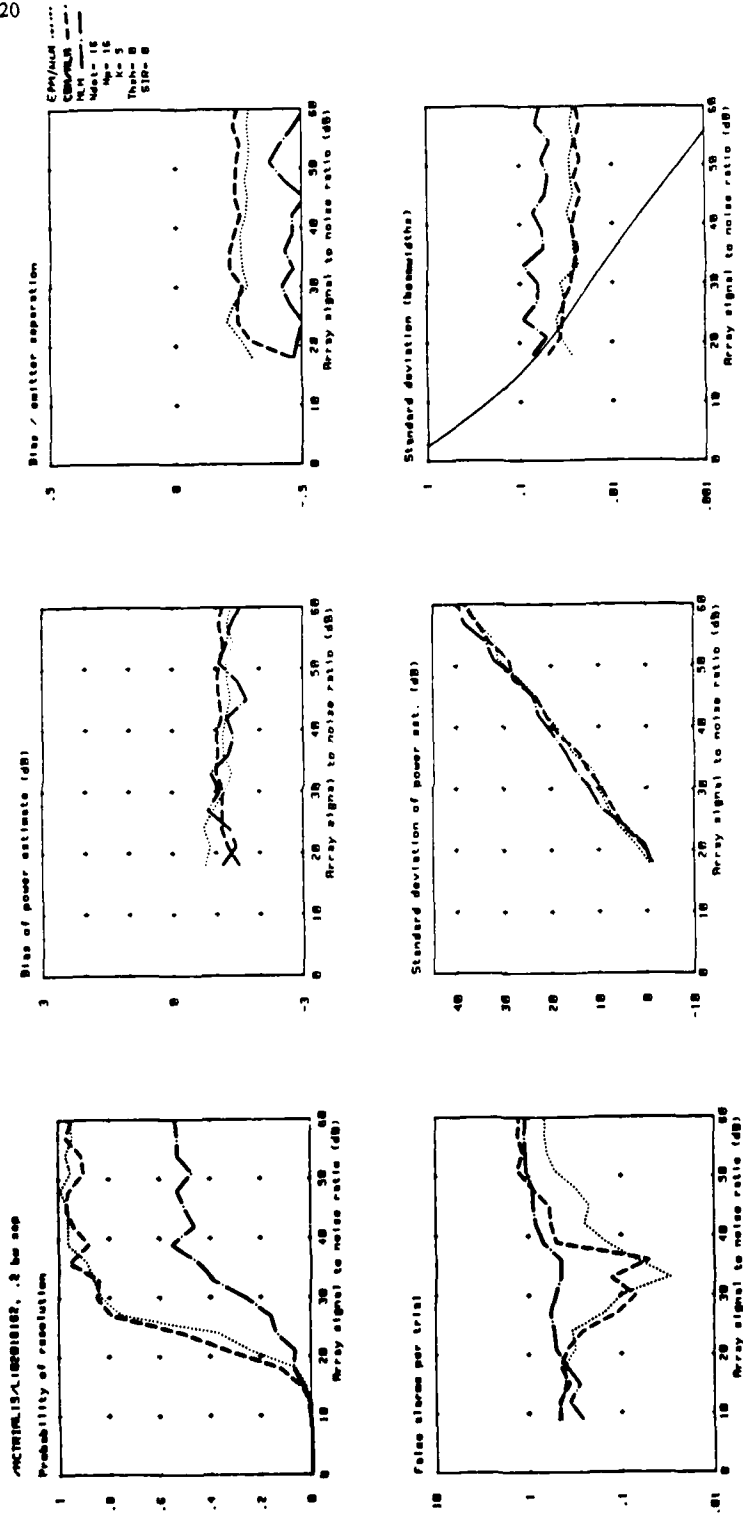


Fig. 14. Performance statistics as a function of array signal to noise ratio (ASNR) for a pair of signals located at 0 and 0.2 beamwidths from broadside. The array calibration is randomly perturbed as shown in Fig. 13. Results are based on 100 trials at each ASNR, taking 16 snapshots of data from the 16 element 0.5 wavelength spaced linear array. Dot-dashed lines show the results of processing using the MLM algorithm, dotted lines show the results obtained using EPM(k=5)/MLM, and dashed lines show the results obtained using CBM(k=5)/MLM. Assumed angle of view from -2 to +2 beamwidths.

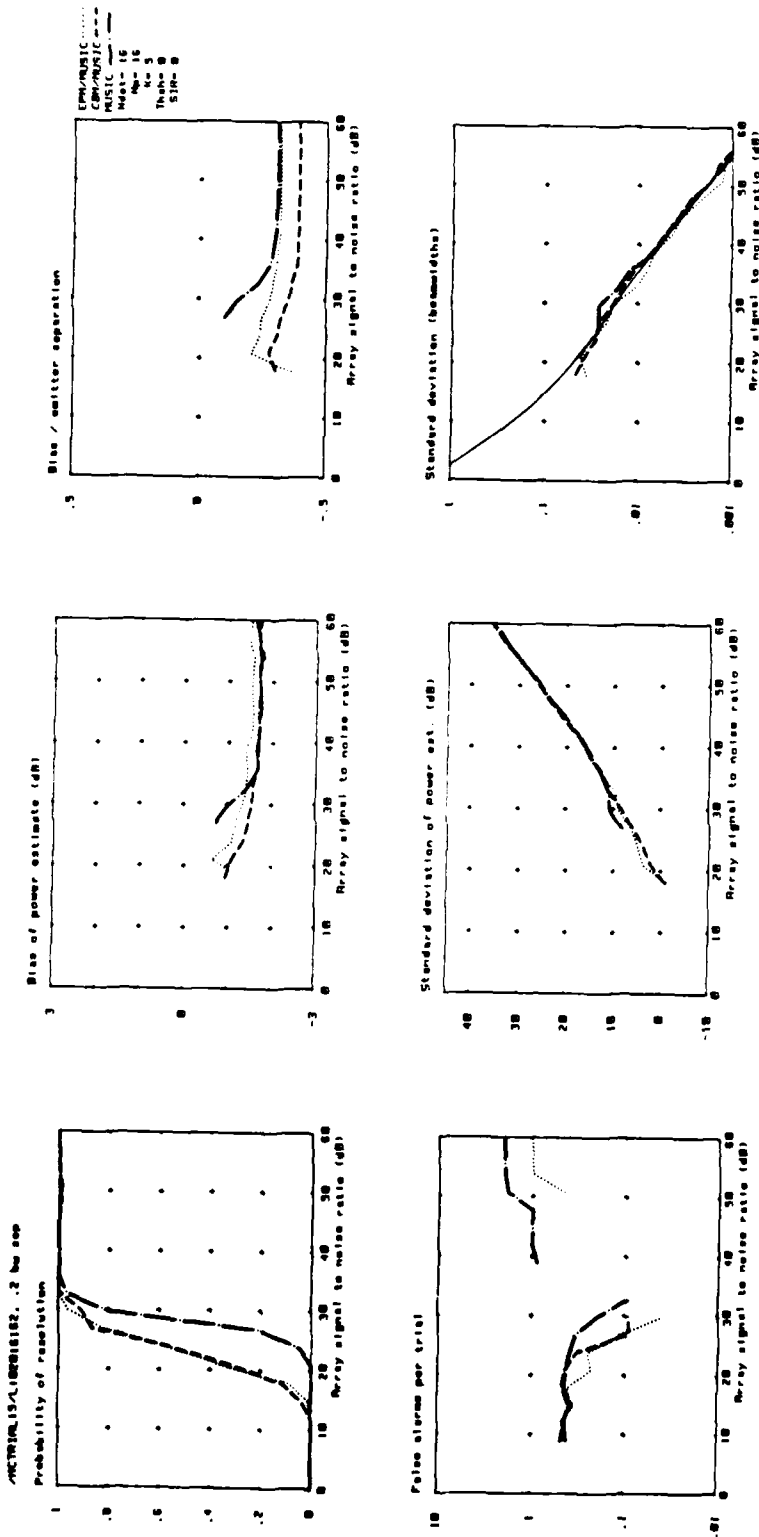


Fig. 15. Performance statistics as a function of array signal to noise ratio (ASNR) for a pair of signals located at 0 and 0.2 beamwidths from broadside. The array calibration is randomly perturbed as shown in Fig. 13. Results are based on 100 trials at each ASNR, taking 16 snapshots of data from the 16 element 0.5 wavelength spaced linear array. Dot-dashed lines show the results of processing using the MUSIC algorithm (equation (9)), dotted lines show the results obtained using EPM(k=5)/MUSIC, and dashed lines show the results obtained using CBM(k=5)/MUSIC. Assumed angle of view from -2 to +2 beamwidths.

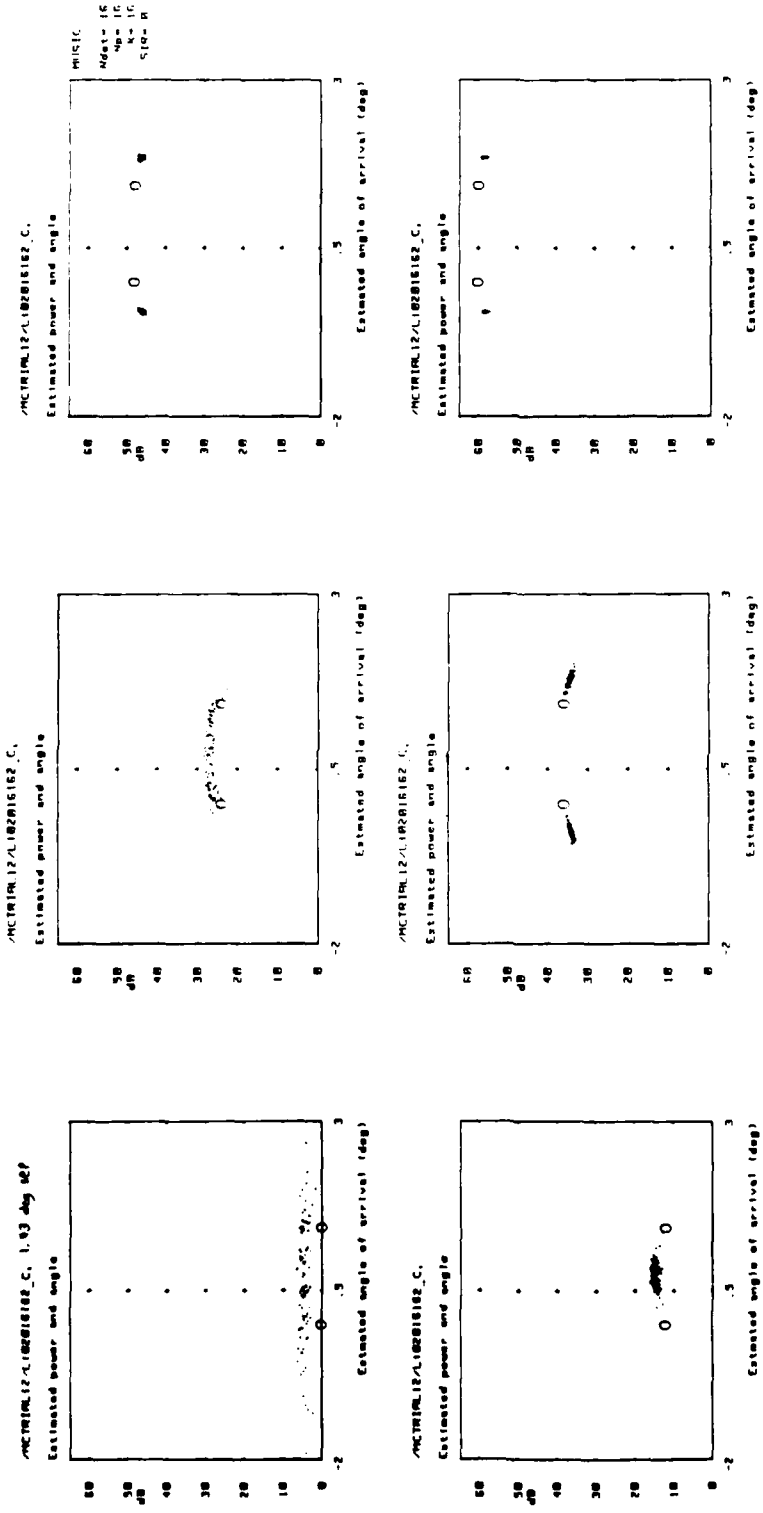


Fig. 16. Scatter diagrams for the MUSIC algorithm in the experiment of Fig. 15. Signal separation of 0.2 beamwidths corresponds to 1.43°. Dots show estimated signal angles and powers for all 100 trials (where these fall within the plotting window) and the two 'O' symbols show the true signal coordinates. Each panel shows results taken for a different ASNR, in the sequence 0, 12, 24, 36, 48, 60dB.

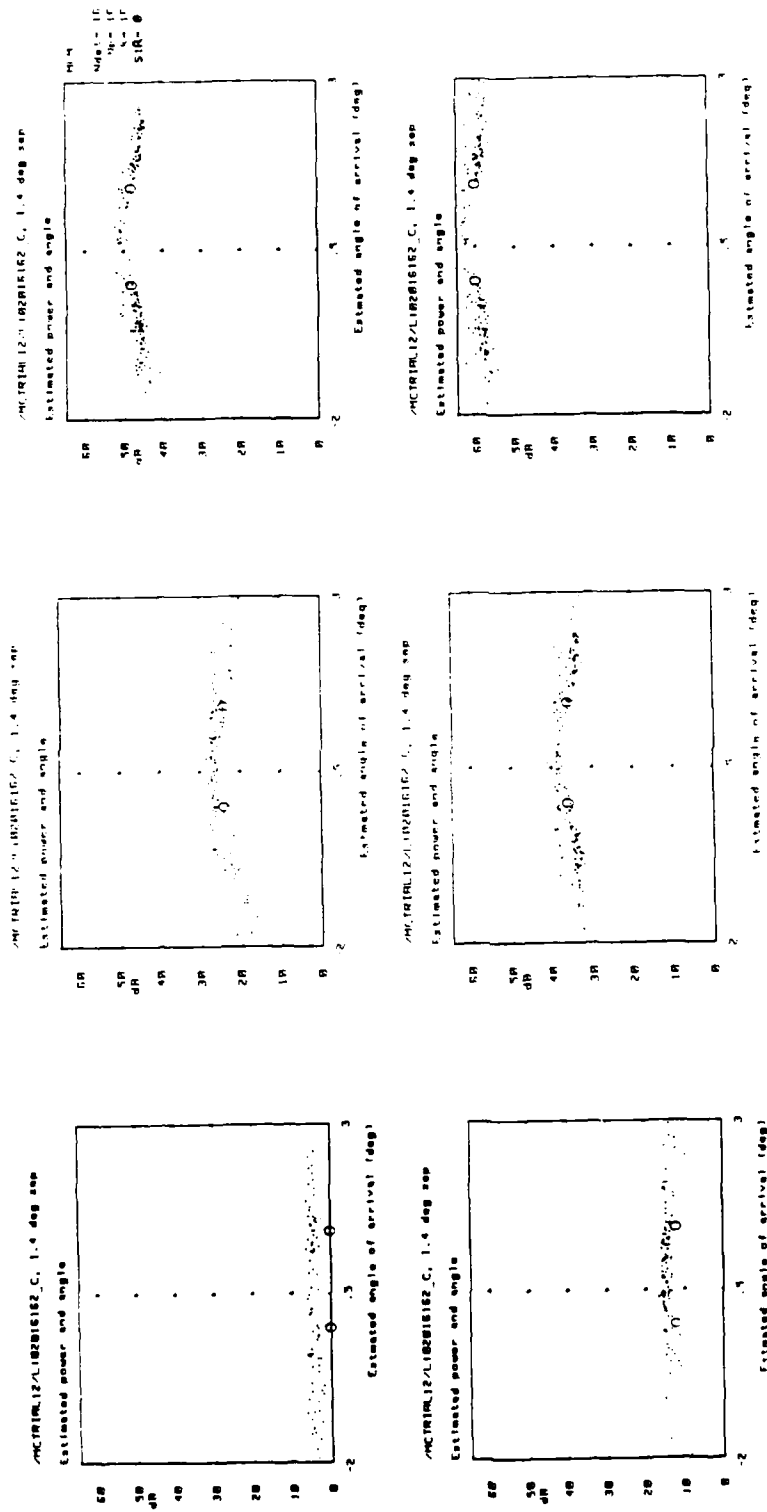


Fig. 17. Scatter diagrams for the MLM algorithm in the experiment of Fig. 14. Signal separation of 0.2 beamwidths corresponds to 1.43°. Dots show estimated signal angles and powers for all 100 trials (where these fall within the plotting window) and the two 'O' symbols show the true signal coordinates. Each panel shows results taken for a different ASNR, in the sequence 0, 12, 24, 36, 48, 60dB.

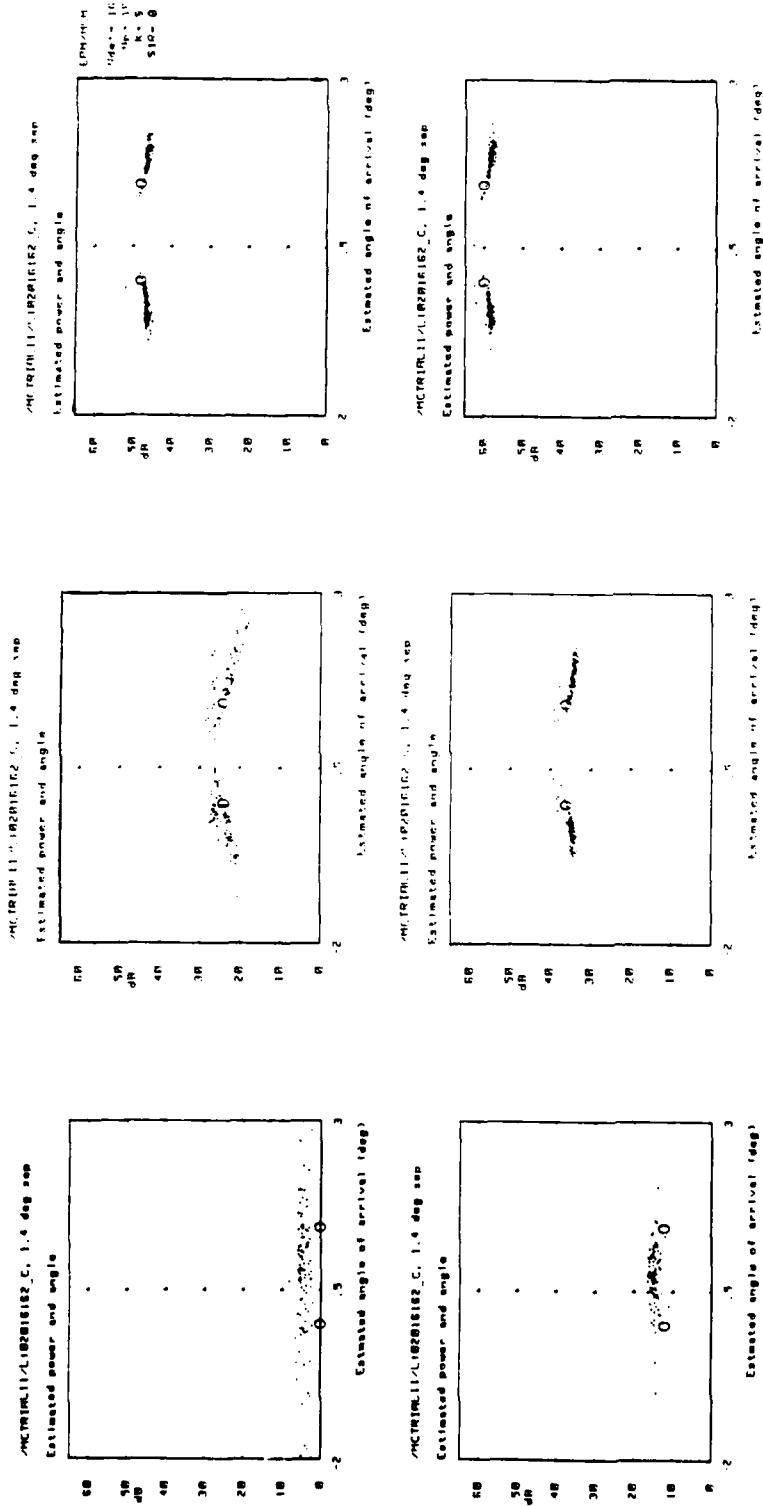


Fig. 18. Scatter diagrams for the EPMMLM algorithm in the experiment of Fig. 14. Signal separation of 0.2 beamwidths corresponds to 1.43°. Dots show estimated signal angles and powers for all 100 trials (where these fall within the plotting window) and the two 'O' symbols show the true signal coordinates. Each panel shows results taken for a different ASNR, in the sequence 0, 12, 24, 36, 48, 60dB.

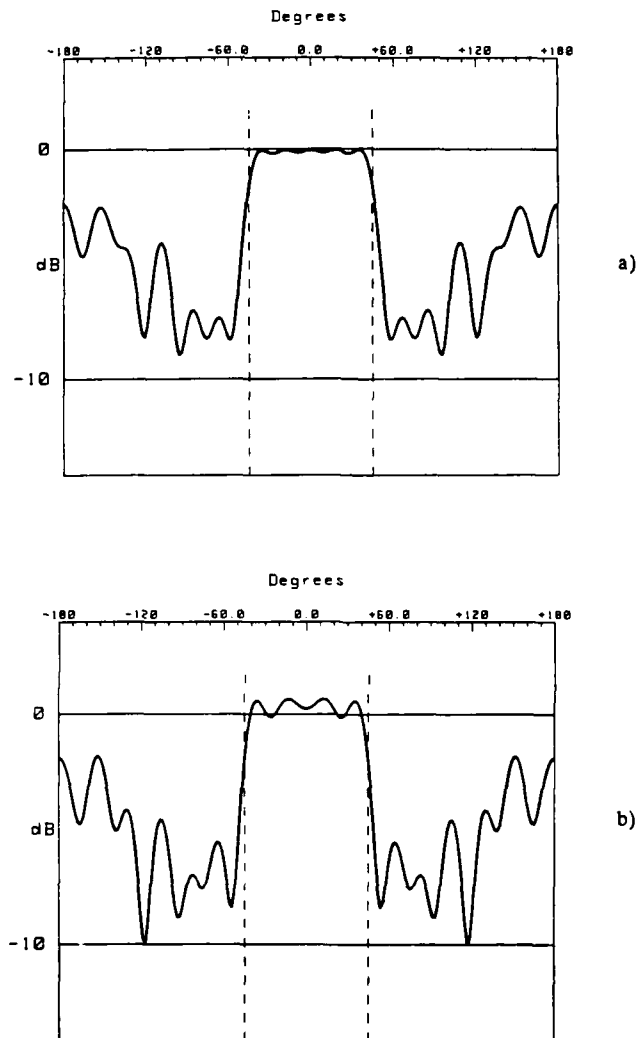


Fig. 19. a) Spatial frequency filter function applied in the plane of the array to data by EPM( $k=5$ ), assuming angular constraints given by  $\sin(\theta_-) = -0.707$  and  $\sin(\theta_+) = 0.707$  (indicated by vertical broken lines) for a 16 element 1.33 wavelength radius circular array. b) Spatial frequency filter function applied to data by CBM( $k=5$ ), for the same array. Beams have been directed at  $18^\circ$  intervals across the desired region.

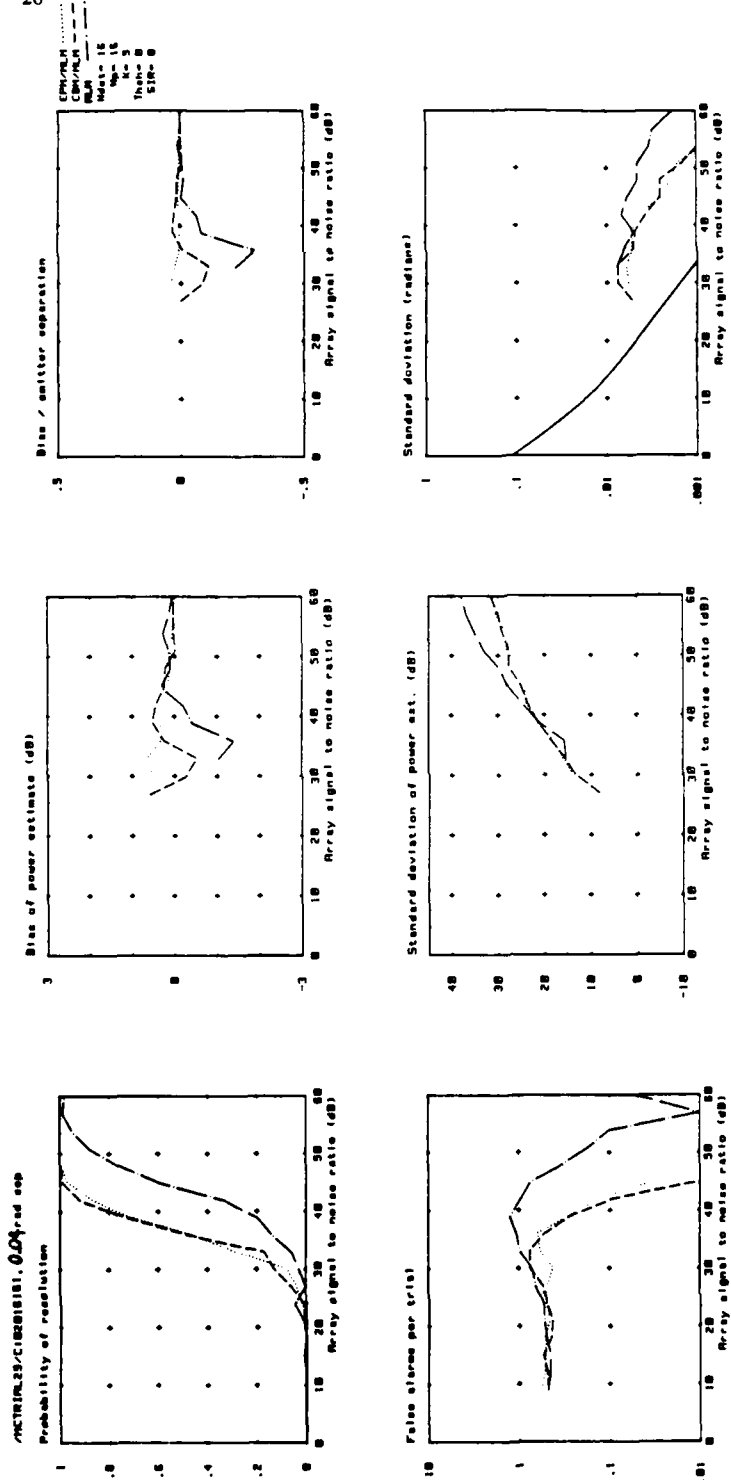


Fig. 20. Performance statistics as a function of array signal to noise ratio (ASNR) for a pair of signals separated by 0.1 beamwidths. Results are based on 100 trials at each ASNR, taking 16 snapshots of data from the 16 elements 1.33 wavelength radius circular array whose beam pattern following EPM and CBM pre-processing is illustrated in Fig. 19. Dot-dashed lines show the results of processing using the MLM algorithm, dotted lines show the results obtained using EPM(k=5)/MLM, and dashed lines show the results obtained using CBM(k=5)/MLM. Assumed angle of view from -2 to +2 beamwidths.

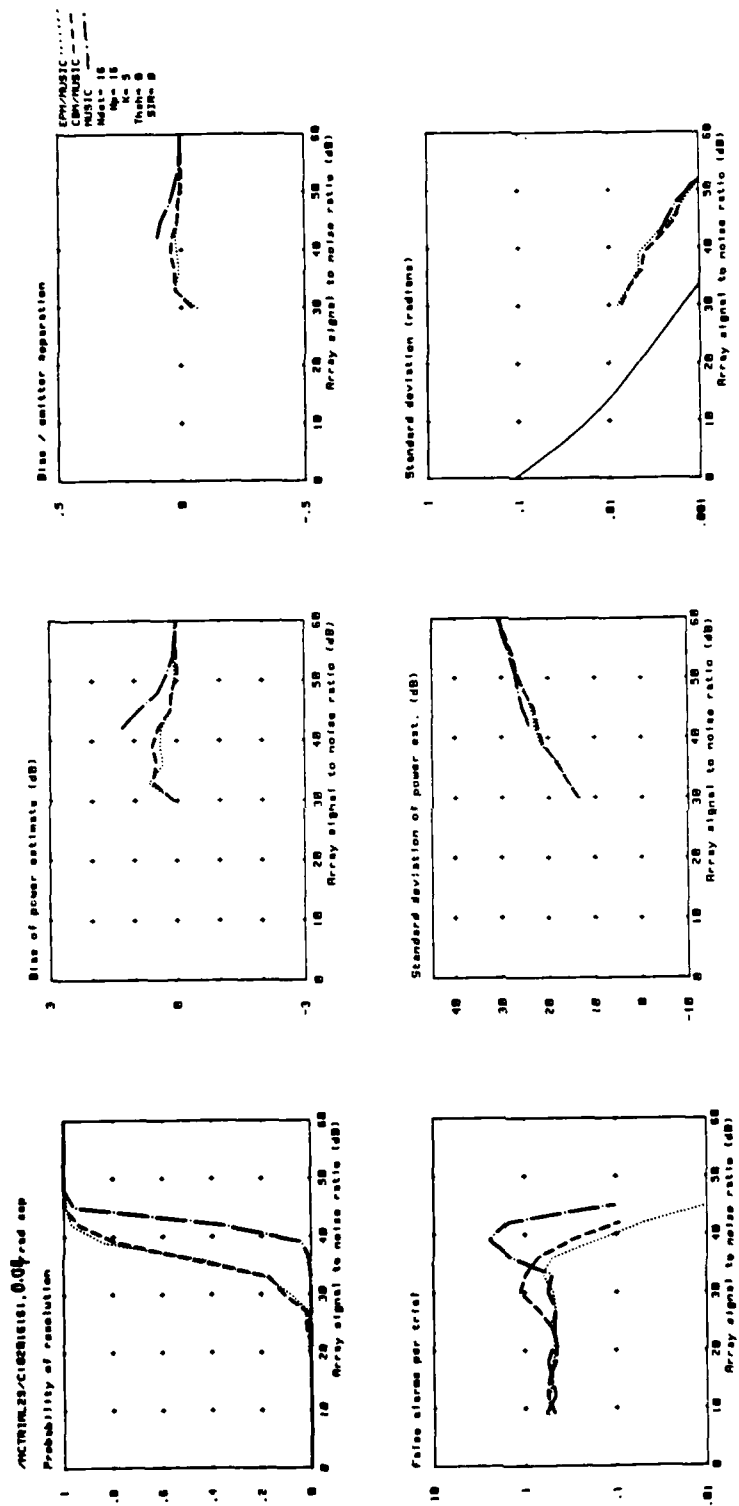


Fig. 21. Performance statistics as a function of array signal to noise ratio (ASNR) for a pair of signals separated by 0.1 beamwidths. Results are based on 100 trials at each ASNR, taking 16 snapshots of data from the 16 element 1.33 wavelength radius circular array whose beam pattern following EPM and CBM pre-processing is illustrated in Fig. 19. Dot-dashed lines show the results of processing using the MUSIC algorithm, dotted lines show the results obtained using EPM(k=5)/MUSIC, and dashed lines show the results obtained using CBM(k=5)/MUSIC. Assumed angle of view from -2 to +2 beamwidths.

## DOCUMENT CONTROL SHEET

Overall security classification of sheet UNCLASSIFIED

(As far as possible this sheet should contain only unclassified information. If it is necessary to enter classified information, the box concerned must be marked to indicate the classification eg (R) (C) or (S) )

1. DRIC Reference (if known)	2. Originator's Reference MEMO 4304	3. Agency Reference	4. Report Security U/C Classification	
5. Originator's Code (if known) 7784000	6. Originator (Corporate Author) Name and Location ROYAL SIGNALS AND RADAR ESTABLISHMENT ST ANDREWS ROAD, GREAT MALVERN WORCESTERSHIRE WR14 3PS			
5a. Sponsoring Agency's Code (if known)	6a. Sponsoring Agency (Contract Authority) Name and Location			
7. Title BEAMFORMING PRE-PROCESSORS FOR HIGH DISCRIMINATION ALGORITHMS				
7a. Title in Foreign Language (In the case of translations)				
7b. Presented at (for conference papers) Title, place and date of conference				
8. Author 1 Surname, initials MATHER J L	9(a) Author 2	9(b) Authors 3,4...	10. Date 1989.08	pp. ref. 27
11. Contract Number	12. Period	13. Project	14. Other Reference	
15. Distribution statement UNLIMITED				
Descriptors (or keywords)				
continue on separate piece of paper				
Abstract High discrimination algorithms based on numerical techniques such as eigen analysis are currently being considered for use in future antenna array systems. In addition to being computationally expensive, such algorithms are only able to achieve significantly enhanced within-beam resolution at high signal to noise ratios. However, if the detected signals are found only within a limited frequency range of region of space, or if the data is oversampled, a pre-processing transform may be applied to the data. This leads to a reduction in the size of the data matrix, enables subsequent processing to be accelerated and lowers the threshold signal to noise ratio required for within-beam resolution. In the spatial domain, the pre-processor is a beamformer. A previous memo has shown how this may be designed using singular vectors of the array calibration matrix. In the current document it is demonstrated by Monte Carlo trials that similar results may be obtained using a conventional beamformer.				